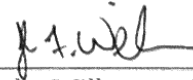Investigation into Alpha Particle Backgrounds in the MAJORANA DEMONSTRATOR

By
John Nance

Senior Honors Thesis
Physics and Astronomy
University of North Carolina at Chapel Hill

2017

Approved:

Dr. John Wilkerson, Thesis Adviser

Dr. Louise Dolan, Reader

Dr. Arthur Champagne, Reader

I. Abstract

Questions about the neutrino's mass and nature have developed into an important area of modern physics research. While neutrino oscillations have shown that neutrinos have non-zero mass, their absolute mass has yet to be determined. Additionally, since they possess no charge, it is possible that neutrinos are Majorana particles, meaning that they are indistinguishable from their antiparticle. The MAJORANA DEMONSTRATOR (MJD) aims to probe the neutrino's absolute mass, and its Majorana nature by searching for neutrinoless double-beta decay (0υββ). Backgrounds from alpha particles potentially pose a problem to this experiment. Alpha particles are produced from elements in the 238-uranium (^{238}U) and 232-thorium (^{232}Th) decay chains, and although alpha particle energies are typically higher than the 0υββ Q-value, they can lose energy before entering the active mass of the detector, and deposit energy near the 0υββ Q-value. Initially, the dependence of alpha rates on detector geometry is explored. Then, two studies conducted on data collected by MJD are presented, one looking for correlations between observed alpha rates and detectors' processing history and manufacturing date, and the other looking for alpha-alpha and beta-alpha coincidence events in the ^{238}U and ^{232}Th decay chains. No correlation is found between a detector's processing history and its alpha rate, but a detector's age shows a weak negative correlation with alpha rate, suggesting the decay of plated out radon progeny. Results of the coincidence study do not provide strong evidence of the presence of ^{232}Th or ^{238}U signatures in MJD data.

II. Introduction

A. Neutrinoless Double-Beta Decay

The observation of neutrino oscillations has shown that neutrinos are not massless, but there is still much we do not know about them. Two of the most important characteristics of neutrinos currently under investigation are their absolute mass, and whether they are a Majorana fermion. In order to be a Majorana fermion, the particle must be its own antiparticle. Most particles, like electrons, have

antiparticles with opposite charge, such as the positron. Since neutrinos carry no electric charge, it is possible that they could be Majorana fermions. If true, this would imply lepton number violation[1], and could provide possible scenarios to account for the matter-antimatter asymmetry in the universe[2,3}.

The only viable method of determining whether neutrinos are their own antiparticle is the observation of neutrinoless double-beta ($0\nu\beta\beta$) decay. In normal beta decay, a nucleon decays, emitting an electron and a neutrino. Some atoms are energetically forbidden from undergoing single beta decay, but have been observed to undergo two neutrino beta decay, like 76-germanium (^{76}Ge), which has a Q-value of 2039 keV. Two neutrino beta decay ($2\nu\beta\beta$) simply refers to a process in which two beta decays happen simultaneously in the same nucleus, emitting two electrons and two neutrinos. In $2\nu\beta\beta$ decay, the energy of the reaction is shared between the emitted electrons and neutrinos, resulting in a broad spectrum of electron energies. If the neutrino is indeed its own antiparticle, then $0\nu\beta\beta$ decay would also be possible. In this process, two nucleons decay as in $2\nu\beta\beta$, but no neutrinos are emitted. This is because the antineutrino emitted by one nucleon is absorbed by the other nucleon. For $0\nu\beta\beta$ decay, the entire decay energy is carried off by the two electrons, leading to a single detectable energy of 2039 keV. Observation of this process would be direct evidence that the neutrino is its own antiparticle.

B. The MAJORANA DEMONSTRATOR

The MAJORANA Collaboration aims to probe the Majorana nature of the neutrino using the MAJORANA DEMONSTRATOR (MJD). MJD is an array of 44.1 kg of high purity germanium (HPGe) detectors, located 4850 feet underground at the Sanford Underground Research Facility (SURF). The goal of this experiment is to demonstrate that a low enough background level can be achieved to justify building a tonne-scale experiment. The detectors used in MJD are p-type point contact (PPC) detectors, which have several useful characteristics. The electrical field and corresponding weighting potential in PPC detectors results in relatively long drift times for holes created throughout the bulk of these detectors, with a rapid increase in weighting potential near the point contact. This allows for

discrimination between the signal shapes of single-site and multi-site events. 0νββ decay is a single-site event, so the use of PPC detectors enables one to cut out background multi-site events and focus on the signal of interest. Of the detectors used, 27.9 kg are enriched, meaning that they have been enriched to 88% in ^{76}Ge. The remaining detectors are natural, composed only of natural germanium (7%). In the DEMONSTRATOR, the HPGe detectors are used as both the source and detector for 0νββ decay.

For ^{76}Ge, the region of interest (ROI) for 0νββ decay is 2039 +/- 2 keV. In order to detect this decay, which has an estimated half live of greater than 10^{25} years, the level of background in the 0νββ ROI must be as low as possible. The goal of MJD is to achieve a background level of 3 counts per tonne of material per year, in the ROI. MJD implements several measures to reduce background, focusing on using ultra-clean materials, shielding, and pulse shape analysis cuts of data. The detectors are assembled into detector units (DU), which are built using electroformed copper and PTFE components inside a nitrogen purged glovebox. The detector units are then combined into strings consisting of stacks of 3 – 4 detectors. Seven strings are placed within an electroformed copper cryostat, named a module, which is then placed inside a shield of low-background copper. MJD operates two modules. The ultra-clean materials used in MJD have much lower levels of inherent radiation, specifically of the radioactive elements ^{232}Th and ^{238}U. These two elements are a large source of background because their decay chains, shown in Appendix 1, contain many radioactive elements that emit alpha and beta particles, and gamma rays. In particular, gammas from 208-thallium (^{208}Tl) are a source of background in MJD that must be controlled. They may enter the detector, Compton scatter, then exit the active mass. This can produce single site events with energy inside the 0νββ ROI, which would be indistinguishable from a true 0νββ signal.

Outside the copper cryostat and copper shield, there is a shield of low-background lead (Pb). This protects the detectors from external gammas and x-rays that would obscure the sought after 0νββ signal. The lead shield is surrounded by an aluminum radon enclosure, to keep out radon-containing air

from the lab. Finally, cosmic ray muons are detected using plastic scintillator veto panels outside the

radon enclosure and neutrons are absorbed using a layer of polyethylene. The placement of the

experiment 4850 feet underground also greatly reduces cosmic ray background. Once data are

collected, pulse shape analysis (PSA) and pulse shape simulations (PSS) are used to better understand

and cut out events that are not of interest, such as multi-site events.

C. Alpha Particle Backgrounds

Alpha particles are a source of background in MJD. These particles are produced with energies

ranging from 3.9 to 8.8 MeV. While this is above the 0νββ Q-value, it is possible for alpha particles to

lose energy before entering the detector, then to deposit energy within the ROI in the active region.

This energy loss can occur in the parts surrounding the detector, known as the external bulk, or in the

dead layer of the detector itself.

HPGe detectors have three
types of surfaces, the n+ contact, p+
contact, and the passivated surface.
The n+ and p+ contacts are used for
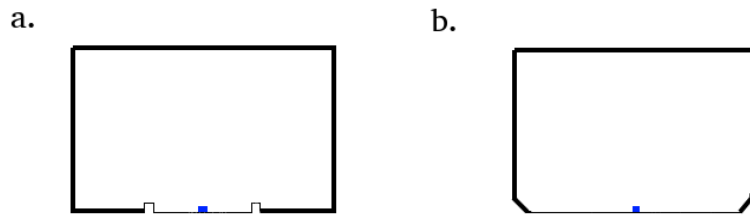biasing and signal connection. The
n+ layer is composed of diffused

Figure 1: Side view of MJD detectors. The thick line is the n+ surface, and the thin line is the alpha susceptible passivated and p+ surface. The small blue point on each is the point contact. a. represents the natural detectors, and b. represents the enriched detectors

lithium ions, with a thickness of 0.5-1mm, and the p+ layer is composed of implanted boron ions, with

a thickness of approximately 0.5μm. This layer is inactive, meaning that energy deposited in this layer

is not observed in the detector signal. The n+ layer is too thick for alpha particles to penetrate, so a

detector's susceptibility to alpha background depends on the surface area of its p+ layer and passivated

surface, both of which are thin enough for alphas to penetrate. For the two types of cylindrical PPC

detectors that MJD uses, the n+ contact covers most of the detector, leaving only a small circular region

of p+ where the point contact is made, and the bottom of the detector where there is a passivated

surface, which is alpha-susceptible. A side view of MJD detectors is shown in Figure 1. This smaller alpha-susceptible surface area gives the PPC detectors another advantage over n-type detectors. Additionally, this small region also limits the directions that alphas originating away from the detector's surface can be incident from.

D. ^{238}U and ^{232}Th Decay Chains

Alphas originating from radon (Rn) progenies are especially important to consider because of the possibility of radon plate out onto surfaces on and around detectors when these materials are exposed to air containing radon. Two of the most common isotopes of radon are ^{222}Rn, part of the ^{238}U decay chain, and ^{220}Rn, part of the ^{232}Th decay chain. Both of these isotopes eventually decay into a stable form of lead (Pb), but along the way they decay into radioactive forms of Pb, polonium (Po), and bismuth (Bi), transitions that emit alpha particles of various energies. These radon progeny can attach or implant onto detector surfaces, and become sources of alpha backgrounds[4]. As an example, consider the decay chain of ^{222}Rn, which eventually arrives at ^{210}Pb. ^{210}Pb decays to ^{210}Bi, then to ^{210}Po, which emits a 5.3 MeV alpha[4]. The 22 year long half life of ^{210}Pb means that if this isotope was implanted onto any surface near a detector, it would be a long lived source of alpha background[4, 5]. It is in order to mitigate these effects that the parts used in MJD are stored in nitrogen purged dryboxes before use, and detector strings and cryostats are built within nitrogen purged gloveboxes. See Appendix 2 for related work at UNC.

E. Estimating Potential Surface Alpha Backgrounds

In [6], a charged-ion interaction model was used to characterize the energy loss of alphas traversing a HPGe detector's surface and to estimate the potential backgrounds from alpha particles deposited on the surface of detectors. Using this model, along with a nuclear physics simulation software, MaGe, the efficiency for a surface alpha decay to deposit energy within the 4 keV 0νββ ROI

was determined to be $1.47 \pm 0.004(stat)^{+0.10}_{-0.20}(sys) \times 10^{-5}$ [6]. The alpha background rate was calculated using the following formula:

$$R_\alpha = \frac{k}{M} \int_S A(\vec{r}) \epsilon(\vec{r}) \Omega(\vec{r}) dS \qquad (1)$$

where M is the mass of the detector in kg, A is the surface alpha activity in Bq/cm2, ϵ is the previously determined efficiency, and Ω is the solid angle of the alpha susceptible area with which the area element dS has direct line of sight, in this case the p+ area. The coefficient

$k = 3.154 \times 10^{10} \frac{kg * s}{tonne * year}$ changes the background rate from counts per kilogram-second into

counts per tonne-year. When only considering surface decays, the formula simplifies to:

$$R_\alpha = k \frac{S}{M} A_{avg} \epsilon \qquad (2)$$

where S is the susceptible surface area, and A_{avg} is the average surface activity rate. The background rate on the p+ contact of the natural detectors used in MJD was calculated using a mass of 0.579 kg and a surface area of 0.2 cm^2, resulting in a value of $R = 1.57^{+0.16}_{-0.17} \times 10^5 A_{avg}$, where the average activity depends on the surface alpha activity in the current location. The results of this calculation are shown for various detectors and exposure activities in Table 1.

Source	Activity (Bq/cm²)	Background Rate (counts in ROI/t-y)	
		P-PC (Natural)	N-type
Clean room	1.0 x 10⁻⁶	0.16	70
MJ BG model	5.0 x 10⁻⁷	0.08	35

Table 1: The estimated surface alpha background count rate for natural P-PC detectors, like those used in MJD, and for typical n-type detectors, calculated in [6]. These rates are based on two assumed alpha surface-activity levels, that of a class-100 clean room used in the Borexino experiment[4], and that of the MJD background model.

These results indicate that the alpha backgrounds in the ROI for the natural MJD detectors should be negligible, under these exposure assumptions. However, as will be discussed in Section III, the enriched MJD detectors have a much larger passivated surface, and this study will be extended.

F. MJD Data Set 1

This investigation into alpha background will focus on MJD's data set 1 (DS1). Data taking for DS1 took place from December 31st 2015, to April 14th 2016. This time span is 104 days, but this is not the value used as the livetime in calculations of rates. Some data were rejected due to high external radon presence, commissioning tests, or calibration runs. Table 2 shows the breakdown of how data are classified in DS1.

Total	104.68 days
Total Acquired	97.52 days
Physics	54.73 days
High Radon	7.32 days
Disruptive Commissioning Tests	28.61 days
Calibration	6.86 days
Down time	7.16 days

Table 2: DS1 run times[7].

Active Mass (Total)	12.43 +/- 0.2 kg
Active Mass (Enriched)	11.31 +/- 0.17 kg
Active Mass (Natural)	1.12 +/- 0.04 kg

Table 3: The total active mass of DS1, along with the active mass of enriched or natural detectors alone[7].

The livetime used for spectral analysis in DS1 is 54.73 days. Table 3 shows the total active mass of DS1, along with that of the enriched and natural detectors separately. Event counts are converted into rates by dividing the number of counts by the active mass and livetime, resulting in rates of counts/kg/day.

The analysis of DS1 data is done using what are termed skim files. After data are taken in MJD, the data are processed using the germanium analysis toolkit (GAT), and stored in what are called gatified files. These are very large files and have many parameters for analysis. Skim files are compact versions of these files that hold fewer parameters and have much smaller file sizes, but tag events based on analysis and cuts that have been applied to the raw data. These files are analyzed in ROOT, a C++ framework for analyzing nuclear and particle physics data. Through this framework, skim files can be

analyzed by applying cuts. Cuts use the parameters stored in the data files to eliminate or focus on certain data.

G. The DCR Cut

In addition to preventative measures to reduce alpha backgrounds, like using ultra-clean materials and assembly, a method for singling out alpha events in MJD data has been developed. This method is based on a phenomenon known as delayed charge recovery (DCR) that has been observed in HPGe PPC detectors. In these detectors, when an event occurs close to the passivated surface, it is possible for the ionized charge to drift along the detector surface, rather than through the detector bulk, towards the point contact. Monte Carlo simulations of hole drift in HPGe crystals have shown that charges move 10 to 100 times slower when drifting along the surface[8]. This slow drifting leads to identifiable characteristics in the alpha associated signal, leading to a change in the slope of the signal's tail. This different slope can be used as a means to cut, or conversely to focus on, only DCR signals in MJD data[9]. The range of typical alpha particles in germanium is less than 20μm, so almost all external detectable alphas will occur on the passivated surface or pass through the surface, making them much more likely to induce DCR signals than other interactions[10].

In Section III the observed alpha rates in DS1, as determined by the DCR cut will be compared to expected rates using the model discussed in Section II-E. Then in Section IV an investigation will be conducted using MJD data and the DCR cut, along with detector records, to look at the dependence of alpha rates for individual detectors on detector unit components, and whether high alpha rates can be attributed to a detector's processing history or age. Finally, in Section V, the presence of coincidence events in MJD data will be investigated as possible indicators of ^{238}U or ^{232}Th progeny.

III. Estimation of Potential Alpha Rates in PPC Detectors

Building upon the work in [6], the expected surface alpha background rates are calculated for both the p+ contact and the passivated surface combined, for both natural and enriched PPC detectors.

Using equation (2), and the detector characteristics given in Table 4 along with the previously

calculated efficiency for surface alpha decay to deposit energy in the 0νββ ROI, the surface alpha

background rates were calculated to be $R = 2.896 \pm 0.009 \times 10^6 A_{avg}$ counts/tonne/year for natural

PPC detectors, and $R = 1.305 \pm 0.027 \times 10^7 A_{avg}$ counts/tonne/year for enriched PPC detectors. Using

those activity dependent formulas, the background rates for each type of detector at two different

surface alpha activity levels were calculated, and are shown in Table 5.

Detector	Mass (kg)	Surface Area (cm²) Total (Passivated + p⁺)
Natural PPC	0.621	3.897
Enriched PPC	0.847	23.85

Table 4: The average mass and combined passivated and p+ surface area for the natural and enriched detectors used in MJD.

Source	Activity (Bq/cm²)	Background Rate (counts in ROI/t-y)	
		Natural	Enriched
Clean room	1.0 x 10⁻⁶	2.896	13.05
MJ BG model	5.0 x 10⁻⁷	1.448	6.525

Table 5: The surface alpha background rates in the 0νββ ROI for the natural and enriched detectors used in MJD. As in the data from [6], the surface alpha activities from a class-100 clean room and the MJD background model are used.

The surface alpha background rate calculated using the combined surface area of the passivated

and p⁺ surface is 18.1 times larger than the background rate calculated in [6] for the same surface alpha

activity. This difference is due to the fact that the combined passivated surface and p⁺ surface of the

natural PPC detectors is approximately 18 times larger than the p⁺ surface alone. Enriched detectors

were not considered in [6], so there is no value to compare the 6.525 counts/t-y to. Both of these

background rates are much lower than 35 counts/t-y alpha background of typical n-type detectors, but

they are still significant considering the MJD background goal of 3 counts/tonne/year in the 0νββ ROI.

Plots of DCR events per detector were produced using data from MJD's DS1. These are

displayed in Figure 2. Using DS1 data and the DCR cut, the actual alpha rates for MJD detectors were
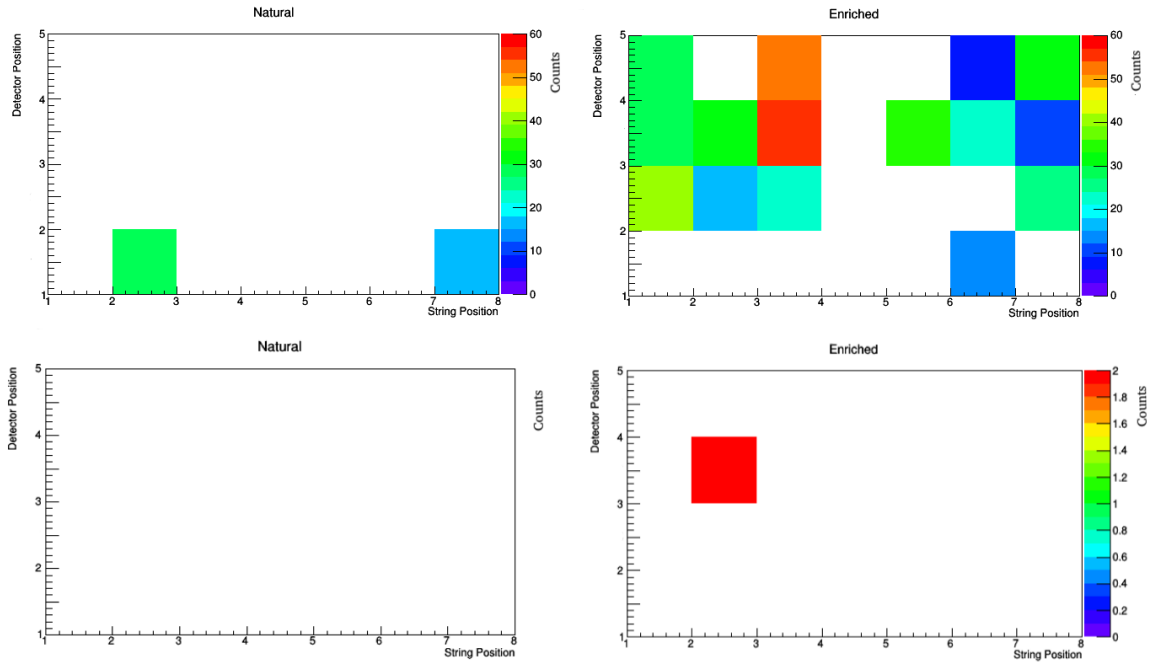
Figure 2: These plots compare DCR events between natural and enriched detectors, sorted by detector. The top plots are for the energy range 400 to 6000 keV. Most enriched detectors registered more DCR events than the two natural detectors. The bottom plots are DCR events within the 4 keV 0νββ ROI, from 2037 to 2041 keV. Within the ROI, only 2 DCR events were found in enriched detectors and zero in natural detectors.

calculated. Table 6 compares the observed alpha rates in DS1 to the calculated surface alpha

background rates in the 4 keV 0νββ ROI.

Detector	Surface alpha background rate (counts/kg/day)	Observed DS1 Alpha Rate (counts/kg/day)
Natural	3.967×10^{-6}	0
Enriched	1.787×10^{-5}	3.231×10^{-3}

Table 6: This table compares the surface alpha background rates in the 0νββ ROI to the observed alpha rates in MJD's DS1.

There were no DCR events within the 0νββ ROI detected by natural detectors in DS1, and only

2 detected by enriched detectors. These values were converted into the units counts/kg/day by dividing

the number of events detected by the livetime of DS1, 54.73 days, and their corresponding active

masses, in Table 3. The rates listed in Table 5 were converted from counts/tonne/year into

counts/kg/day by dividing the rate by the constant k, then multiplying that value by 86400, the number

of seconds in a day. Comparing the values predicted by the surface alpha model and the observed

values, the observed rate in natural detectors is lower, as it is 0. This is to be expected, as there are only 2 active natural detectors in DS1, and the probability of them detecting a DCR event within a 4 keV ROI is small within the 54.73 day livetime. The enriched detectors found 2 DCR events within the ROI, resulting in a rate of $3.231*10^{-3}$ counts/kg/day, two orders of magnitude higher than the predicted $1.787*10^{-5}$ counts/kg/day. Because the substantial energy degradation of alphas originating on the passivated surface was not assumed in [6], it is not useful to directly compare the values determined there and those calculated here. The MAJORANA background model predicts a contribution of 1.370 * 10^{-7} counts/kg/day in the ROI from surface alphas[11], four orders of magnitude lower than the observed alpha rate in DS1. The DCR cut is very efficient, and in this study, the DCR cut was used to single out alpha events. Use of the cut in the opposite way, to cut out only DCR events, allows MJD to eliminate the higher than expected background from alpha events.

IV. Investigation of Individual Detector Rates

A. Hot Detectors

Currently, MJD has collected five sets of data, DS0 through DS4. Using this data, the rate of DCR (alpha) events for each detector in each data set was calculated[12]. In looking at the distribution of rates across all the detectors, shown in Figure 3, detectors with alpha rates greater than 0.2 counts/day were designated "hot" detectors. It was found that of the detectors classified as hot, almost all of them were consistently hot in each data set that they operated in[12]. This suggests that there is something unique about these detectors, how they were handled during fabrication, or the materials surrounding them, that is producing a relatively high number of events that are tagged by the DCR cut. The intent is to test the hypothesis that there may be a correlation between the processing history of these hot detectors, or of the hardware surrounding them, and their high alpha rates.

For the two types of cylindrical PPC detectors that MJD uses, the n+ contact covers most of the detector, leaving only a small circular region of p+ where the point contact is made, and the bottom of the detector where there is a passivated surface, which is alpha-susceptible. This helped narrow the choice of materials to i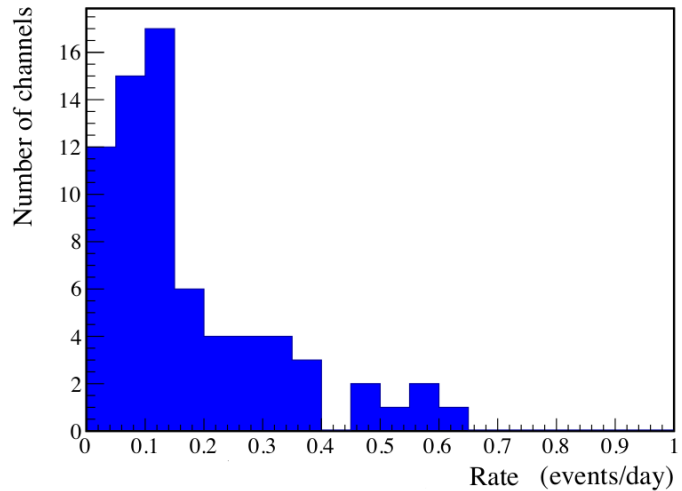nvestigate for correlations between alpha rates and hardware processing. Along with the detector crystals themselves, the pieces of hardware that are investigated here include the contact pins, center bushings, crystal mounting plates, and crystal insulators, all of which, because of their location within the detector unit, have line of sight to the alpha susceptible surface. An MJD detector unit is displayed in Figure 4.
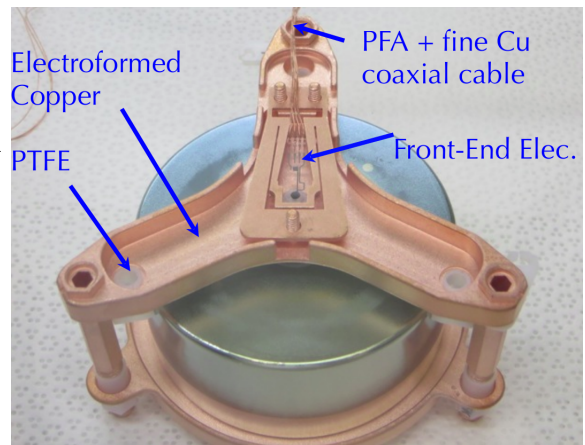

Figure 3[12]: The distribution of alpha rates of MJD detectors. Number of channels is equivalent to number of detectors. Detectors with rates above 0.2 counts/day are designated as hot.

Figure 4: A photograph of the underside of an MJD detector unit.

B. Methods

A spreadsheet was created listing each detector and its corresponding alpha rate by data set, along with an average alpha rate across all data sets. Then, columns were created corresponding to each of the pieces of hardware of interest and the detector crystals. In this investigation, the primary focus was on the amount of time that these pieces of hardware were stored, between various stages in their manufacture, and the assembly of their corresponding detector unit. Time is a useful variable to consider because it can shed light on the presence of radon or its progeny at different stages of detector unit processing, by comparing these elements' half-lives to patterns seen in alpha rates. Any

correlations found among these variables could suggest that alpha emitting isotopes were present in the location of their storage or manufacture. The variables being tested for each piece of hardware are listed below. In addition to these variables, the date of crystal manufacture is investigated, along with the amount of time the detector spent between its removal from the manufacturer's cryostat (de-cryostating) and its assembly into a detector unit.

Contact Pin: Days between tin dipping and DU build (Stored in dry box).

Center Bushing: Days between leaching and DU build (Stored in dry box).

Crystal Mounting Plate: Days between etching and DU build (Stored in dry box).

Crystal Insulators: Days from outgassing to DU build (Stored in dry box).

De-cryostat Date: Days between detector de-cryostating and DU build (Varying storage).

Total Age: Days between the detectors manufacture and DU build (Varying storage).

The correlation coefficient (R) between each detectors values for these variables and each detector's average alpha rate was calculated, and alpha rate was plotted over each of these variables. Results are shown in Table 7 with plots for contact pins in Figure 5, center bushings in Figure 6, crystal mounting plates in Figure 7, crystal insulators in Figure 8, detector de-cryostating in Figures 9 and 10, and detector total age in Figures 11 and 12.

Hardware Piece	Correlation Coefficient		
	Module 1	Module 2	Total
Contact Pin	0.594	-0.285	0.050
Center Bushing	0.210	-0.630	-0.028
Crystal Mounting Plate	0.254	-0.261	0.069
Crystal Insulators	0.321	-0.667	-0.136
De-cryostat Date	0.283	-0.430	-0.001
Total Age	-0.235	-0.703	-0.414

Table 7: This table lists the correlation coefficients between the detectors' observed alpha rates and the time between certain processing events for the corresponding piece of hardware, along with the correlation coefficient between the total age of the detector's and their observed alpha rates. The processing events corresponding to each piece of hardware are listed above. A coefficient was calculated for each module separately, and then all detectors combined.
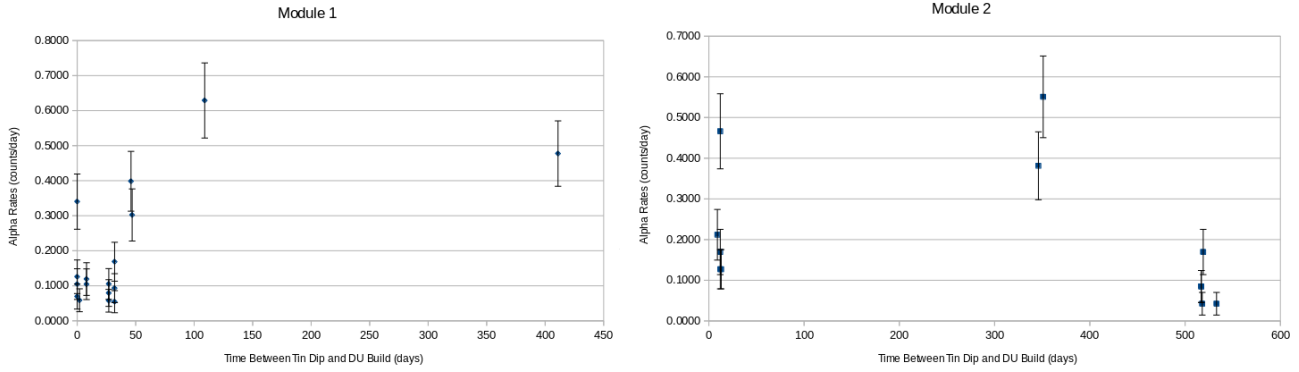
Figure 5: Contact Pin. This figure shows the plots of alpha rate over amount of time that a contact pin spent between its tin dipping and the day its detector unit was assembled. The left plot represents the contact pins from detectors in module 1, and the right represents the contact pins from detectors in module 2.
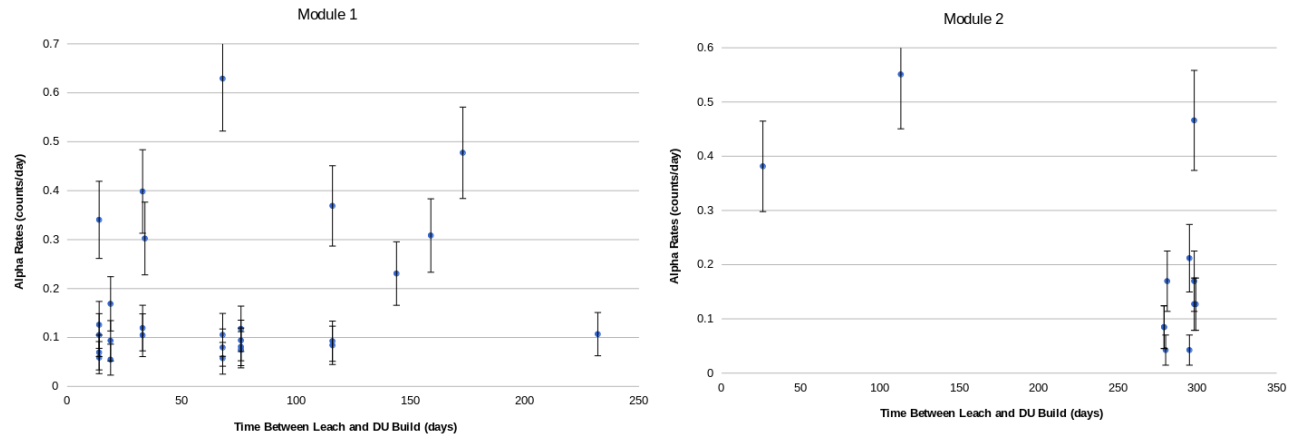

Figure 6: Center Bushing. This figure shows the plots of alpha rate over amount of time that a center bushing piece spent between its leaching and the day its detector unit was assembled. The left plot represents the center bushings from detectors in module 1, and the right represents the center bushings from detectors in module 2.
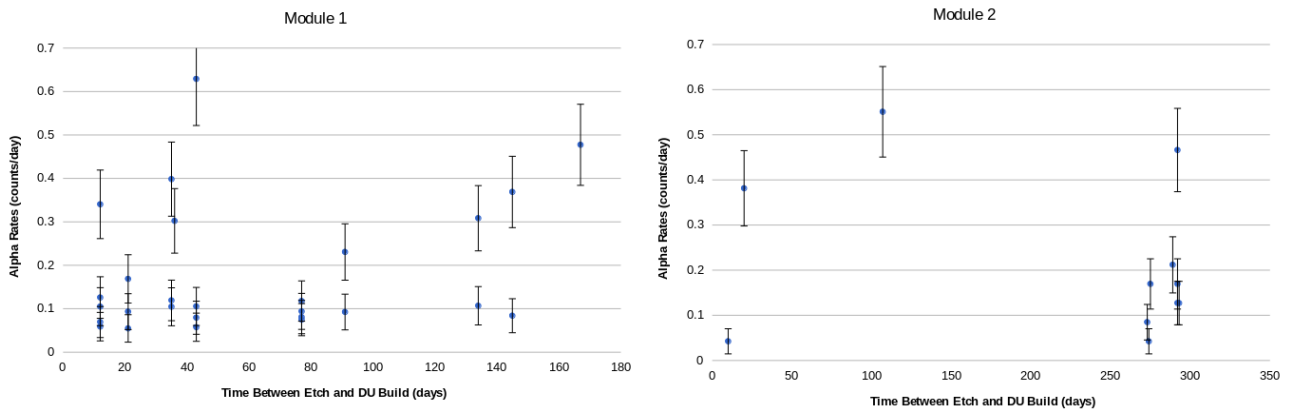

Figure 7: Crystal Mounting Plate. This figure shows the plots of alpha rate over amount of time that a crystal mounting plate spent between its etch and the day its detector unit was assembled. The left plot represents the crystal mounting plates from detectors in module 1, and the right represents the crystal mounting plates from detectors in module 2.
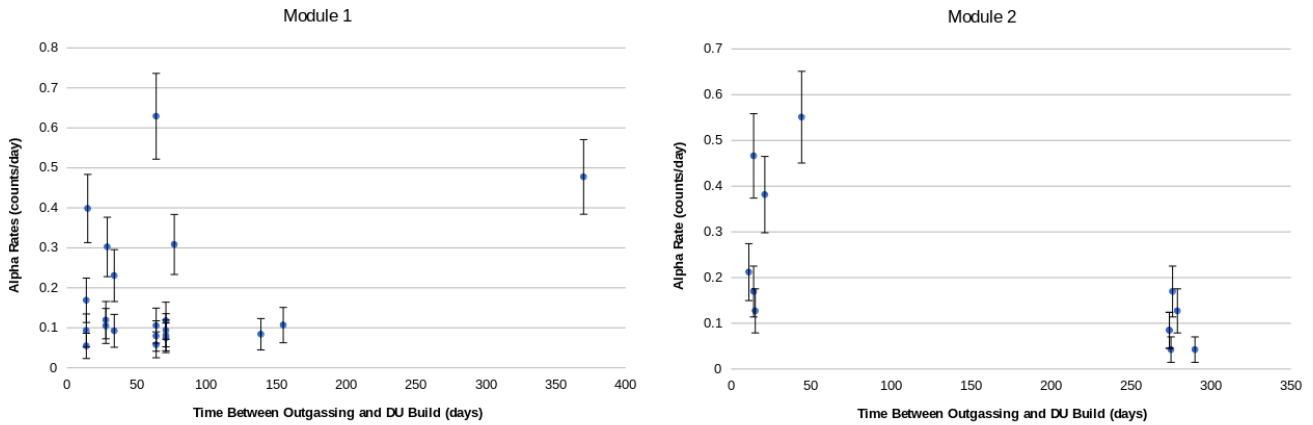
14

Figure 8: Crystal Insulator. This figure shows the plots of alpha rate over amount of time that a crystal insulator spent between its etch and the day its detector unit was assembled. The left plot represents the crystal insulators from detectors in module 1, and the right represents the crystal insulators from detectors in module 2.
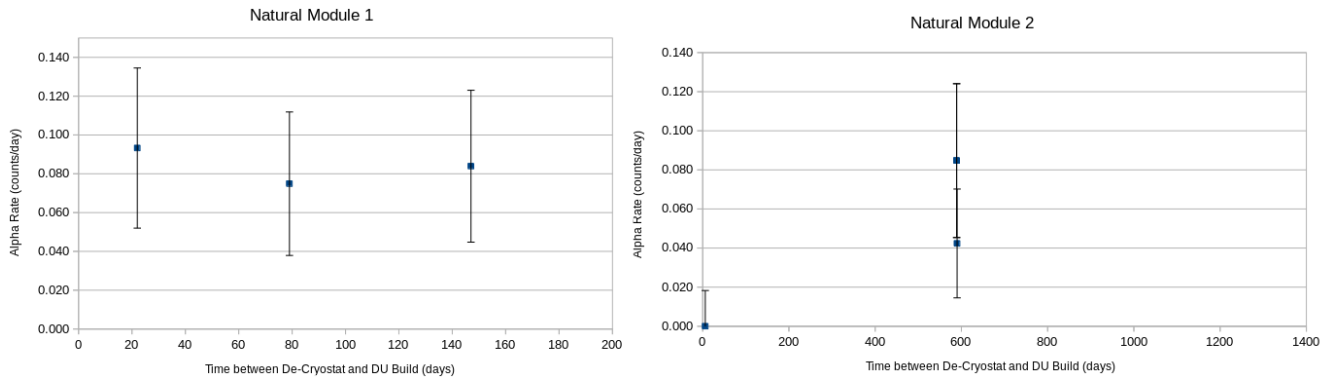

Figure 9: Detector De-cryostat. This figure shows the plots of alpha rate over amount of time that a detector spent between its de-cryostating and the day its detector unit was assembled, for natural detectors. The left plot represents the detectors in module 1, and the right represents the detectors in module 2.
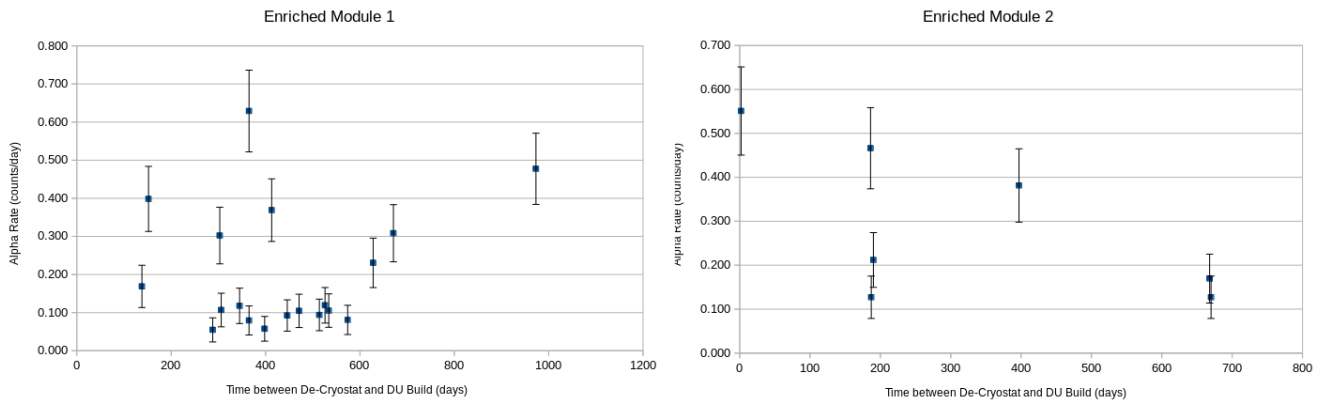

Figure 10 Detector De-cryostat. This figure shows the plots of alpha rate over amount of time that a detector spent between its de-cryostating and the day its detector unit was assembled, for enriched detectors. The left plot represents the detectors in module 1, and the right represents the detectors in module 2.
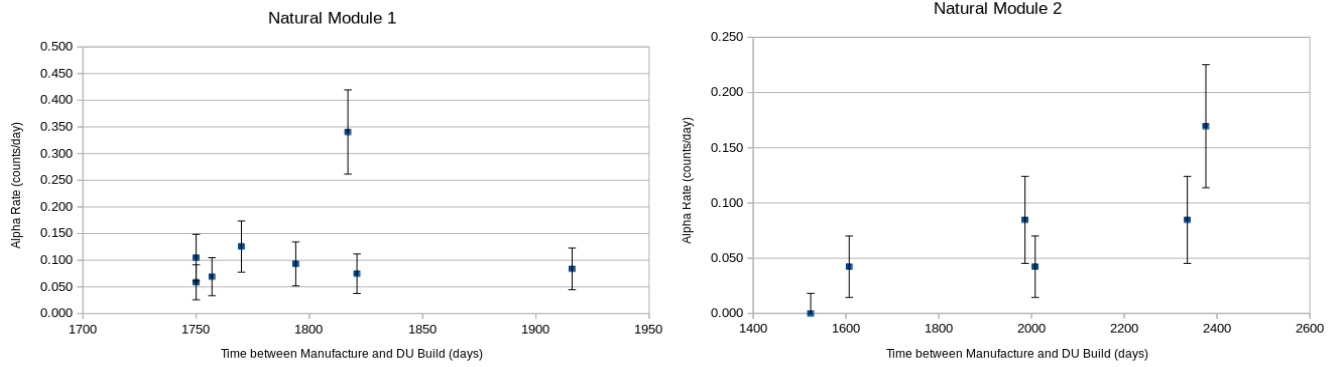
15

Figure 11: This figure shows the alpha rates for natural detectors in MJD plotted against that detector's total age, the time period between its manufacture and its detector unit assembly.
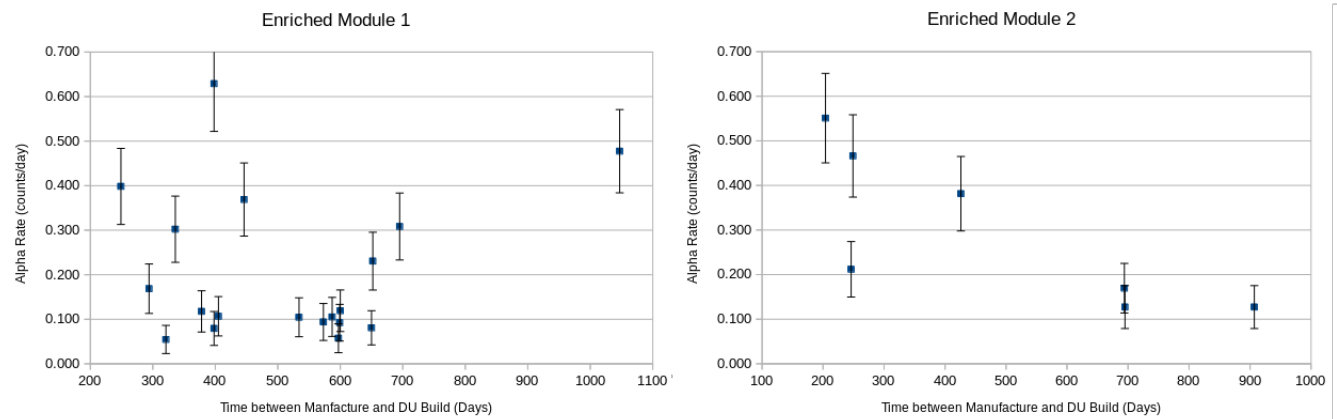

Figure 12 This figure shows the alpha rates for natural detectors in MJD plotted against that detector's total age, the time period between its manufacture and its detector unit assembly.

C. Results

The correlation coefficient R measures the strength of the linear relationship between the two variables used in its calculation[13]. If any of the variables investigated here had any influence on detected alpha rate, one would expect an R value close to either 1 or -1, indicating that the longer a piece was stored between a certain processing event and detector unit build, the higher alpha rate observed in that detector, or an inverse relationship, respectively. In the R values calculated by module in Table 7, there are a few values that stand out, namely the contact pins in module 1, the center bushings in module 2, the crystal insulators in module 2, and the total age of detectors in module 2. Alone, these would merit a further look into possible radon or radon decay products in proximity to

16

these hardware pieces. Positive correlations would indicate radon or its decay products near the part's storage location, as its alpha rate increases the longer it was there. A negative correlation would indicate radon or its decay products in the location that the processing occurred, for example where the outgassing of module 2 crystal insulators occurred. After this processing occurred, the longer the piece was stored, the longer the alpha emitters that plated out on the piece would have to decay away, so that there is less alpha emitting material on the piece during MJD operation. If either of these situations were the case, the correlation in each module should be similar, under the assumption that the hardware used in each module was exposed to the same conditions during processing and storage. Table 7 shows that this is not the case. For each variable investigated, except the detectors total age, the sign of the R value is different in module 1 than it is in module 2, and for each one, the R value in module 1 is positive and in module 2 is negative. Considering all detectors, module 1 and module 2 combined, no variable exhibited even a slight linear correlation of either sign, except detector's total age, with R = -0.414.

A table listing each detector used in this investigation along with their total ages is available in Appendix 3. Considering the detector's total age, both module 1 and module 2 detectors showed a negative correlation between that detector's observed alpha rate and the time between its manufacture and its use. The total R value for detectors in both modules shows a weak negative correlation, meaning the longer a detector spent between its manufacture and its assembly into a detector unit, the lower the alpha rate it measured in operation. Of the two types of detectors used, the natural detectors were all manufactured over a period of 909 days from the years 2009 to 2011, whereas the enriched detectors were manufactured over a period of 843 days over the years 2012 to 2015. The R values for the natural and enriched detectors separately were calculated and are shown in Table 8.

Correlation Coefficient	Module 1	Module 2	Total
Natural	0.127	0.838	0.244
Enriched	0.091	-0.795	-0.216

Table 8: The correlation coefficients between total detector age and observed alpha rates, for natural and enriched detectors in module 1 and module 2.

	Natural	Enriched
Standard Deviation in Age (days)	250.0	205.3
Average Manufacture Date	01/04/10	11/04/13

Table 9: This table shows the standard deviation between detector ages for natural and enriched detectors, along with the their average manufacture dates.

For the natural detectors, module 1 has a very weak positive correlation, while module 2 has a strong positive correlation, which could indicate that the natural detectors used in module 2 may have been exposed to radon decay products during storage. The enriched detectors in module 1 show no correlation, but in module 2 they show a strong negative correlation, which could indicate that alpha emitting isotopes plated out onto these detectors decayed away during storage. The correlation coefficients for both natural and enriched detectors in both modules show very weak linear correlations, in opposing directions. When considering all detectors together, they exhibit a slightly stronger negative correlation, -0.414, between age and alpha rate. If there was a source of alpha emitting material that implanted onto the detectors at their manufacture location, the stronger negative correlation when considering both enriched and natural detectors together may be due to the decay of this material over the large time period between the dates of their manufacture. Table 9 lists the standard deviation between detector ages for both natural and enriched, both on the scale of 200 days. On the other hand, the difference between the average manufacture date of the natural and enriched detectors is 1400 days. Looking at the decay chains for ^{222}Rn and ^{220}Rn, every alpha decay has a half-life of 4 days or less, except ^{210}Po and ^{210}Pb, a long lived source of ^{210}Po. In the ^{222}Rn decay chain, ^{210}Po alpha decays into ^{206}Pb with a half-life of 140 days. The standard deviation in age of both types of detectors is slightly less than two ^{210}Po half-lives . Assuming an initial mass M of ^{210}Po plated out on

the detector, after two half-lives, the mass of ^{210}Po left would be approximately $\dfrac{M}{4}$. On the other

18

hand, the difference in the average dates of manufacture of natural and enriched detectors is 1400 days,

or ten ^{210}Po half-lives. This time period corresponds to a decrease in ^{210}Po mass from M to $\dfrac{M}{1024}$. If

detectors were exposed to radon during the manufacturing process and ^{210}Po plated out onto the

detectors' surfaces, most of the ^{210}Po would have decayed from the natural detectors by the time the

enriched detectors were being manufactured, resulting in lower alpha rates for those detectors during

operation, and the observed negative correlation when looking at all detectors together. However, that

explanation assumes that all detectors were exposed to the same conditions during manufacture.

Enriched and natural detectors were manufactured by different companies at different locations,

making it unlikely that they were exposed to the same levels of radon and its products during

manufacture. Additionally, if any ^{210}Pb were implanted onto the detectors, more ^{210}Po would continually

be produced while the original mass was decaying.

The relatively weak R values shown by the hardware pieces investigated, along with the change

in sign of the R value from module 1 to module 2, indicates no clear correlations. The total age of the

detectors, defined as the time between its manufacture and its assembly into a detector unit, showed a

slight negative correlation between age and alpha rate. This could be explained by the introduction of

an alpha emitting material during manufacture, which decays over time before the detector is placed

into the detector unit, as discussed above with ^{210}Po. Confirmation of this hypothesis would require

measurements over a longer time period, as well as a direct comparison between detectors known to

have been exposed to radon and its decay products and those used in MJD. Finally, analysis of DCR

data could be done using fits other than a linear correlation, such as an exponential fit. In the case of an

alpha emitter decaying, its mass decreases exponentially with time, so an exponential fit of the data

collected here would be may produce stronger correlations.

19

A. Coincidence Events

A method of identifying the presence of, and distinguishing between, ^{238}U and ^{232}Th is the presence of coincidence events. A coincidence event is a decay that is followed almost immediately by another decay. These events occur when after one decay, the product of that decay decays again with a very short half life. These events are seen in both ^{238}U and ^{232}Th chains, in both cases in the decay of Bi to Pb, an example of a beta-alpha coincidence. In the ^{238}U chain, ^{214}Bi beta decays to ^{214}Po, which then alpha decays to ^{210}Pb with a half life of 164μs. In the ^{232}Th chain, ^{212}Bi decays to ^{212}Po, which in turn alpha decays to ^{208}Pb with a half life of 0.3μs[14]. In these cases, one would expect to see a beta event, followed by an alpha event only microseconds later. The presence of these beta-alpha coincidences in MJD data could indicate the presence of ^{238}U or ^{232}Th at some time during the MJD production process, and the difference in half life between each can be used to distinguish between them.

B. Methods

In order to search MJD data for beta-alpha coincidences, an iterator in ROOT was used to iterate over every event in MJD's DS1, and a data structure was created to store information about each event as the iteration occurred. This data structure, EventBuffer, stores information about the fifty most recent events, specifically their date, time, energy, the run that they occurred on, and the detector that detected them. Using the ROOT iterator along with the EventBuffer data structure, a script was created to identify coincidence events. For each event in DS1 within a specified energy range, this script checks whether that event is a DCR event, and then looks through all the prior events stored in the EventBuffer for coincidence events.

The way that the script determined whether to count an event as a coincidence was by comparing the recorded time of the alpha event and the earlier event and seeing if the earlier event

occurred at a short enough time before the alpha to be considered a coincidence. In this case, the time requirement was a difference in time between the alpha and earlier event of 36 ms. This time was chosen because it encompasses many half-lives of the beta-alpha coincidence elements of interest, [214]Po from the [238]U chain, and [212]Po from the [232]Th chain, but still maintains a small window in which to search for only coincidence events.

C. Results

Total Events in DS1	5761
Total DCR Events in DS1	916
Total Events With a Coincidence	50
DCR Events With a Coincidence	7
Total DCR Coincidence Events Found	11

Table 10: Listed here are the number of total, DCR, and coincidence events in MJD's DS1 in the energy range 400 to 6000 keV.
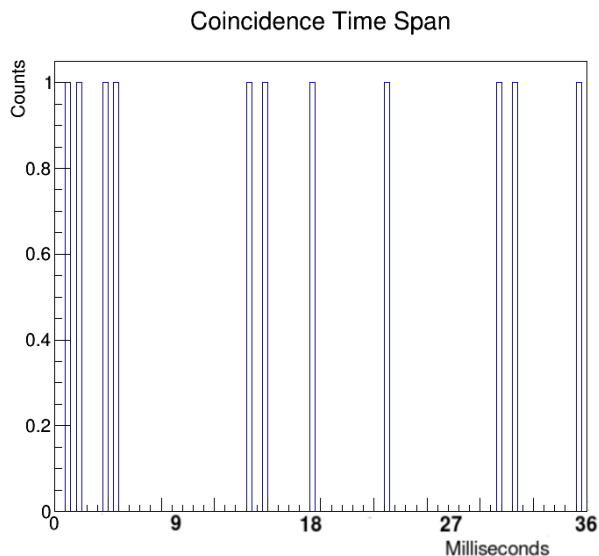

Figure 13: This displays the distribution of time spans between coincidence events and their corresponding DCR event.
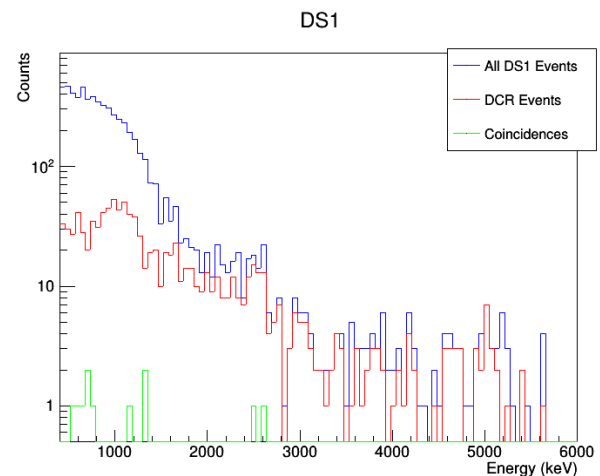

Figure 14: This plot displays the energy spectrums of all DS1 events, DCR events in DS1, and the DCR-associated coincidence events found in DS1.

The statistics found from the coincidence scripts are shown in Table 10. Figure 13 shows the distribution of time spans between the original alpha event and the coincidence event that preceded it. Figure 14 shows a plot of the energy spectrum of coincidence events compared to all DCR events, and all DS1 events.

Table 10 reveals that in the energy range 400 to 6000 keV, DCR events make up 15.9% of all events detected in DS1. Of those DCR events, only 7 were found to have at least one coincidence event, an event prior to them that occurred within the 36 ms time restriction. DCR events with a coincidence make up 14% of all the events found in DS1 to have at least one coincidence. There were 11 coincidence events in total that were associated with a DCR event, meaning that some of the 7 DCR events had multiple events prior to them within the time restriction. In the case when a DCR event has multiple coincidences, only one of those prior events could possibly be due to an actual beta-alpha or alpha-alpha coincidence event. Figure 14 reveals that a majority of the DCR events in DS1 are located at lower energies, with a drop off at 3000 keV. This is similar for coincidence events, they are all present at energies under 3000 keV. This is important because the 4 keV $0\nu\beta\beta$ ROI is located in the region 2037 to 2041 keV, where DCR events make up a majority of the events detected, and above the region of $2\nu\beta\beta$ events, which make up a majority of the DS1 events under 1500 keV.

More than half of the coincidence events occur under 1000 keV, in the approximately 200 keV region from 600 keV to 800 keV. This cluster of coincidence events around that energy region could be a indicator of ^{232}Th. This is because in the beta-alpha decay scheme laid out above for ^{232}Th, ^{212}Bi beta decays to ^{212}Po, which then alpha decays to ^{208}Pb soon after. The Q-value of the beta decay in that case is 2252 keV, but since the average detected energy of beta particles is one third of their Q-value[15], one would expect to detect a value around 750 keV for that decay, on average. In Figure 13, the time between each detected coincidence event and its associated DCR event are plotted. The distribution of times is fairly regular, with a slight majority under 18 ms. This plot does not provide any evidence towards the possibility of ^{232}Th being the source of the coincidences, as ^{212}Po's half-life is 0.3 μs. If those coincidences were all from ^{232}Th, their time distribution would be concentrated near zero on that plot. Further evidence against the hypothesis that these coincidences are due to ^{212}Po is a comparison of the DCR coincidence rate to the overall, non-DCR coincidence rate in DS1. The rate of DCR

coincidences is $\dfrac{7}{916} = 0.008$ coincidences per DCR event, and the rate of non-DCR coincidences is

$\dfrac{43}{4845} = 0.009$ coincidences per non-DCR event. These rates are very close, which suggests that the

DCR coincidence events are not due to ^{212}Po, but are simply accidental coincidences, independent

events that both happen to occur within the time restriction. If the DCR coincidences were due to ^{212}Po,

one would expect the rate of DCR coincidences to be higher than that of non-DCR coincidences.

This study would benefit from expansion to data sets beyond DS1. Inclusion of all 5 currently

available data sets would shed more light on the characteristics of DCR events and coincidences events,

simply by greatly increasing the sample size. This would provide statistics more representative of MJD

data as a whole.

VI. Conclusion

In this investigation into alpha background in MJD, three main areas were analyzed. The first

was the dependence of observed alpha rate on alpha susceptible surface area, which was analyzed by

comparing natural and enriched detectors. Both the calculation and the observed results confirm that a

greater alpha susceptible surface area leads to higher alpha rates, although the observed rates are much

higher than the calculated rates. This is most likely due to the fact that the degree of energy degradation

on the passivated surface that is seen in MJD was not taken into account in the calculations. Next, an

investigation into the possible causes for high alpha rates in some MJD detectors was conducted by

looking for correlations between the amount of time that certain hardware had been stored and the

alpha rates of the detectors they're associated with. No strong correlation was found for any pieces of

hardware, although a slightly negative correlation between the total age of the detector and its alpha

rate was found. This may support the hypothesis that radon decay products plated out on detector

surfaces will decay away over time. Finally, the prevalence of coincidence events in DS1 data was

investigated, and the possibility of ^{232}Th or ^{238}U signatures in the energy spectrum of coincidence events was explored. The cluster of coincidence events around 750 keV, the expected average beta particle energy for ^{212}Bi, may indicate the presence of ^{232}Th, although the distribution of time spans for the coincidence events, and a comparison of DCR and non-DCR coincidence rates, did not provide information to support this.

VII. Acknowledgments

VIII. Appendices

Appendix 1

Element	Type of Decay	Half-life
Uranium 238	Alpha	4.5×10^9 years
Thorium 234	Beta	24.5 days
Protactinum 234	Beta	1.14 minutes
Uranium 234	Alpha	2.33×10^5 years
Thorium 230	Alpha	8.3×10^4 years
Radium 226	Alpha	1590 years
Radon 222	Alpha	3.825 days
Polonium 218	Alpha	3.05 minutes
Lead 214	Beta	26.8 minutes
Bismuth 214	Beta	19.7 minutes
Polonium 214	Alpha	1.5×10^{-4} seconds
Lead 210	Beta	22 years
Bismuth 210	Beta	5 days
Polonium 210	Alpha	140 days
Lead 206	Stable	

Table 11: The decay series of 238-uranium.

Element	Type of Decay	Half-life
Thorium 232	Alpha	14.1×10^9 years
Radium 228	Beta	5.75 years
Actinium 228	Beta	6.13 hours
Thorium 228	Alpha	1.91 years
Radium 224	Alpha	3.66 days
Radon 220	Alpha	55.6 seconds
Polonium 216	Alpha	0.15 seconds
Lead 212	Beta	10.64 hours
Bismuth 212	Alpha (36%) Beta (64%)	60.6 minutes
Polonium 212	Alpha	0.305×10^{-6} seconds
Thallium 208	Beta	3.07 minutes
Lead 208	Stable	

Table 12: The decay series of 232-thorium.

Appendix 2

On site at SURF, after the electroformed copper pieces to be used in construction of MJD are machined, they are stored in nitrogen purged dryboxes. Additionally, all assembly of components used in MJD occurs in nitrogen purged gloveboxes. When assembly takes place, one of these gloveboxes can achieve a particle count on the scale of 10 particles per cubic foot, for 0.3μm particles. The use of nitrogen as a purge gas is essential to creating a low radon environment. Nitrogen is also inert, so it will not react with anything within the chambers. Purging these chambers with nitrogen displaces dust, water, air, and any other undesirable materials, such as radon, that would normally be present.

In the purge system in use at SURF, the purge gas used is boiloff from liquid nitrogen (LN) dewars. It is beneficial to use a liquid nitrogen source because the difference in boiling point between nitrogen and radon guarantee a nitrogen source that is radon free. Nitrogen's boiling point is 77.36 K,

whereas radon's is 211.35 K. While the liquid nitrogen boils off and is directed to the dryboxes and gloveboxes, any radon remains in the dewar in liquid form.

The liquid nitrogen purge system implemented at SURF supplies several chambers with purge gas, and is sourced from a set of two 180 liter LN dewars. The level of LN in each dewar is monitored, and a system is in place which automatically switches which dewar is used as the supply depending on how much LN each contains. It is desirable to implement a simpler, smaller scale LN purge system at the University of North Carolina at Chapel Hill (UNC), where current upgrades of cables and connectors for the MAJORANA DEMONSTRATOR is underway, so that components can be assembled under conditions similar to those at SURF. Using the schematic and parts list for the LN purge system at SURF as a reference, a purge system for use at UNC was designed. This system uses one 180 liter dewar of LN as its source. From this dewar, LN flows into a customized 50 liter dewar, which has been modified to allow for its use with a level probe and vacuum jacketed vapor withdrawal line. The flow from the source dewar into the customized dewar is controlled by an AMI Level Controller. This device tracks the level of LN in the 50L dewar, and opens or closes the line between this dewar and the source when certain setpoints are reached. The level controller also operates a pressure builder, which is activated when pressure within the 50L dewar is too low. From the 50L dewar, LN boiloff is routed through a heat exchanger, which brings it closer to room temperature, and is then sent to the chambers which it is purging. Flow into each chamber is controlled by flowmeters placed right before the inlet into each chamber. After flowing through the chamber, the purge gas is vented through the lab exhaust. A schematic for this purge system was produced using the xfig drawing program, and is shown below in Figure 15.

This design is a simplification on that used at SURF in the following ways. Only one source dewar is used, so there is no switching system in place to alternate the source between multiple dewars. The level controller in the UNC purge system only controls one solenoid valve, between the source

26

dewar and 50L dewar. At SURF, the 180L dewars supply LN for multiple purposes, so the level controller controls multiple valves, and has two responses for a HIGH level reading in the 50L dewar. At the lower HIGH setpoint, the level controller closes a valve that only blocks the 50L dewar. At the higher, emergency HIGH setpoint, the level controller shuts off the LN source completely. Finally, the system planned for use at UNC is designed only to purge up to three chambers, whereas the system at SURF can purge up to nine chambers.

After completion of the design and schematic, a bill of materials was created, and a failure modes analysis review meeting was held. In this meeting, all conceivable modes of failure for the UNC purge system were discussed and given a rating based on their likelihood and severity. Parts for construction of this system are currently awaiting order once project funds are received.
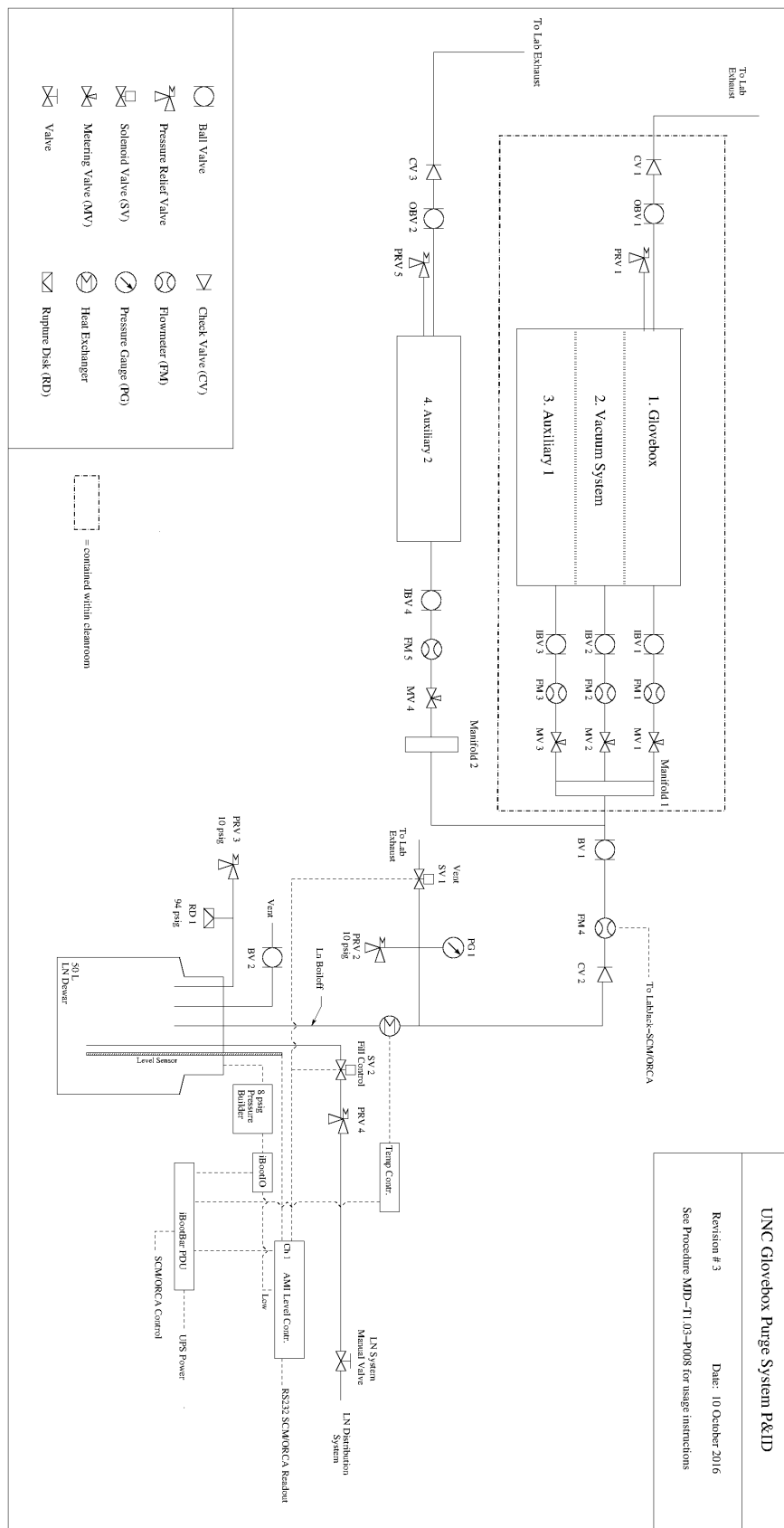
Figure 15: A schematic of the LN purge system designed for use at UNC.

Appendix 3

Detector Serial Number	Total Age (Days)	Detector Serial Number	Total Age (Days)
B8474	1794	P42662C	321
B8480	1937	P42698A	405
B8455	1817	P42538B	1047
B8470	1750	P42573A	695
B8463	1770	P42575B	599
B8465	1757	P42661A	446
B8469	1750	P42573B	652
B8477	1916	P42574C	587
B8482	1821	P42661B	398
B8487	1524	P42574A	597
B8459	2104	P42662A	398
B8481	2336	P42574B	573
B8576	2008	P42662B	378
B8594	1986	P42537A	650
B8595	2003	P42665B	686
B8461	2422	P42664B	484
B8607	1971	P42748B	425
B8456	2433	P42748A	426
B8621	1960	P42749A	695
B8466	2376	P42749B	694
B8473	2363	P42853A	385
B8487	1932	P42853B	204
B8619	1972	P42712A	570
B8717	1607	P23517A	907
P42698B	249	P42909B	249
P42575A	534	P42909C	249
P42661C	336	P42665C	879
P42538A	600	P42712B	789
P42664A	321	P42909A	246
P42665A	294		

Table 13: This table displays the total ages for each detector used in the individual detector investigation section. The detectors with serial numbers beginning with "B" are natural detectors, and those beginning with "P" are enriched detectors.

IX. References

[1] J. Schechter and J. W. F. Valle, "Neutrinoless double-β decay in SU(2)×U(1) theories," Physical Review D, vol. 25, no. 11, pp. 2951–2954, 1982

[2] M. Fukugita and T. Yanagida, "Barygenesis without grand unification," Physics Letters B, vol. 174, no. 1, pp. 45–47, 1986.

[3] P. Di Bari, "An introduction to leptogenesis and neutrino properties," Contemporary Physics, vol. 53, no. 4, pp. 315–338, 2012.

[4] M. Leung, The Borexino Solar Neutrino Experiment: Scintillator Purification and Surface Contamination, Ph.D. Thesis, Princeton, 2006.

[5] L.C. Stonehill, Deployment and Background Characterization of the Sudbury Neutrino Observatory Neutral Current Detectors, Ph.D. Thesis, University of Washington, 2005.

[6] R. A. Johnson, et al., Nucl. Instr. and Meth. in Phys. Research A 639, (2012) 51-58.

[7] C. Cuesta, Run selection and data cleaning of DS1 (P3KJR), (2016).

[8] P. Mullowney, et al., Nuclear Instruments and Methods in Physics Research A 662 (2012) 33–44.

[9] J. Gruszko, (2016), Delayed Charge Recovery Discrimination of passivated surface alpha events in P-type point-contact detectors, University of Washington, Seattle, WA.

[10] Berger, M J, et al. 2005 ASTAR [Online] Available: http://physics.nist.gov/Star.

[11] C. Cuesta, et al., Background Model for the MAJORANA DEMONSTRATOR, (2016) arXiv:1610.01146.

[12] J. Gruszko, Alpha Rate K-S Tests & Rates by Detector, MAJORANA COLLABORATION, (2017).

[13] Correlation Coefficient, MathBits, [Accessed Apr 1 2017], https://mathbits.com/MathBits/TISection/Statistics2/correlation.htm

[14] R. B. Galloway, Uranium and thorium series determination in natural samples by a beta-alpha coincidence technique, (1990), 725-730.

[15] Radiation Safety Manual Radioisotopes, Environmental Health and Safety, [Mar 29 2017],

http://www2.bakersfieldcollege.edu/erp/Radiation/chp4.htm